Imaging of G protein-coupled receptors in solid-supported planar membranes at the single molecule level

Iwan Märki[a], Marcel Leutenegger[a], Matthias Geissbühler[a], Rudolf Robelek[b], Eva-Kathrin Sinner[c] and Theo Lasser[a]

[a] Ecole Polytechnique Fédérale de Lausanne, Lausanne, Switzerland;
[b] Universitiy of Regensburg, Regensburg, Germany;
[c] Max-Planck-Institut für Polymerforschung, Mainz, Germany

ABSTRACT

Odorant receptors are an excellent example of natural superiority in specifically binding specific, small and hydrophobic molecules. They are of particular interest in the development of a sensor platform for G protein-coupled receptors (GPCRs). Odorant receptors (OR5) of *Rattus norvegicus* were incorporated into model membranes by *in vitro* synthesis and vectorial incorporation for achieving natural receptor function. The vectorial insertion of OR5 into the planar membrane and their lateral distribution, their interactions and their mobility within the membrane are of great importance for ligand–receptor interaction. We applied total internal reflection fluorescence (TIRF) microscopy and image analysis to assess the insertion and the OR5 distribution as well as the lateral mobility of these receptors at the single molecule level. The vectorial incorporation of OR5 into planar lipid membranes was investigated with TIRF microscopy and image segmentation. With increasing expression time, the OR5 incorporation density and aggregation increased linearly by about $0.02\mu m^{-2}min^{-1}$. The expression and incorporations of single OR5s were completed within about 8 minutes. The mobility of the incorporated receptors was measured with fluorescence correlation spectroscopy (FCS) and fluorescence recovery after photo-bleaching (FRAP). These measurements revealed that the incorporated receptors were immobilized with this class of lipid membranes.

Keywords: Biomedical imaging, single molecule detection, fluorescence spectroscopy.

1. INTRODUCTION

Membrane proteins are important in medicine and life science and play a fundamental role in cell signalling and transmembrane transport. However, membrane proteins such as G protein-coupled receptors (GPCRs) require a lipid bilayer membrane for a correct folding, i.e. a vectorial incorporation for full receptor functioning is mandatory. The common approach of synthesis in a living cell followed by isolation and reincorporation into a model system is complicated, if not impossible, because the functional structure of the protein is likely to be disordered, incomplete or even destroyed. GPCRs are particularly difficult to isolate as a functioning protein, as improper folding already affects their ability of recognizing ligands. Recent advances in synthetic biology by Robelek et al.[1,2] avoid the isolation issue by an *in vitro* expression process of membrane proteins in the presence of model membranes. Thereby, the proteins are continuously incorporated into the model membranes and correctly folded during their expression.

Robelek et al.[2] observed the vectorial and functional incorporation of OR5 in a solid-supported tethered lipid membrane (tBLM). OR5 is an odorant receptor from *Rattus norvegicus* belonging to the vast GPCR family. The incorporation and orientation of the protein was shown by immunolabeling in combination with surface plasmon enhanced fluorescence spectroscopy (SPFS) and reversible ligand binding was shown by surface-enhanced infrared reflection absorption spectroscopy (SEIRAS). Receptor activation, i.e. upon ligand binding, is of primary interest in cell signalling and signal

Send correspondence to Marcel Leutenegger: marcel.leutenegger@a3.epfl.ch

transduction. In general, the activation event itself and the conformation change of the receptor cannot be measured because this would very likely inhibit the receptor function. But based on induced events in the signalling cascade, a few methods for measuring the activation of GPCRs were developed. For instance, Heyse et al.[3] and Bieri et al.[4] observed the dissociation of the G protein from solid-supported membranes upon photo-activation of incorporated Rhodopsin, which led to a mass change measurable with surface plasmon resonance. In addition, several investigations showed that receptor-ligand binding considerably slows down the diffusion of these receptors, which is in general attributed to an aggregation of GPCRs (homo- or hetero-polymerization) in the cell membrane to launch the signalling cascade. For instance, Lill et al.[5] investigated the signalling kinetics of the neurokinin 1 receptor (NK1R). Initially, this receptor was found to diffuse either fast ($D \approx 0.21\mu m^2/s$) in domains of $\varnothing 1.1\mu m$ or slow ($D \approx 0.011\mu m^2/s$) within domains of $\varnothing 180nm$, but to slow down significantly within 1s after signalling.

We applied total internal reflection fluorescence (TIRF) microscopy and image analysis to assess the insertion and the OR5 distribution, as well as the lateral mobility of these receptors. Whereas SPFS and SEIRAS measure the average signal from an area of a few mm^2, TIRF imaging allows localization and detection of single OR5 receptors in the membrane. The aim of this investigation is to detect receptor-ligand binding by monitoring the lateral mobility of OR5 receptors in these artificial membranes (c.f. the review on FCS studies in model membranes by Kahya and Schwille[6]).

2. MATERIALS AND METHODS

Figure 1 outlines the platform for dual-color FFS measurements in the evanescent field created by TIR at the coverslip–sample interface.[7] It provides TIR fluorescence microscopy and dual-color confocal FFS measurements as well (c.f. thesis chapt. 3 by Leutenegger for further details[8]). Two ps diode lasers provide linearly polarized beams with 635nm and 467nm center wavelengths, respectively. The laser powers are controlled by neutral density filters in addition to the control setting of the laser driver. The beams are passed through polarization maintaining fibers for cleaning up the lateral beam profile. After collimation to an e^{-2} diameter of $\lesssim$ 2mm (TIRF) or $\approx$ 10mm (confocal), they are aligned coaxially to the microscope objective using two beam steerers. Laser-line clean-up filters ensure well-defined excitation spectra. A dichroic mirror combines the beams and an achromatic lens focuses them into the back-focal plane (BFP) of the high NA (1.45) oil immersion objective, which results in circular areas with e^{-2} diameters of $\approx 16\mu m$ (blue) and $\approx 20\mu m$ (red) at the coverslip–sample interface. In the BFP, a lateral offset of the beam foci of $\approx$ 2.3mm results in a super-critical angle illumination, i.e. in an evanescent field excitation.

The sample is mounted on a 150μm thick glass coverslip, which is positioned with a *xyz*-translation stage. In this epi-illumination setup, the fluorescent light is collected with the same high NA objective and focused directly onto the active areas of $\varnothing 50\mu m$ of the single photon detectors. For TIRF imaging, a flip mirror redirects the fluorescence light on a sensitive electron-multiplying CCD camera.

Figure 2 outlines the solid-supported tBLM assembly with an incorporated OR5 receptor. The tBLM was prepared on a thin chromium-gold layer of 5.0nm thickness. The receptor was expressed with a vesicular stomatitis virus (VSV) affinity tag at one terminal. This VSV tag served as target for immunolabeling with a fluorescently labeled antibody. This antibody was labelled with two Cy5 fluorophores (average, inferred from FCS of a 5nM antibody solution). In contrast to the SPFS measurements, no secondary antibody was required due to the higher detection sensitivity. To probe the orientation of inserted OR5 proteins, cDNA constructs with alternative positions for the tag sequence were used: one cDNA coded for a C-terminal VSV affinity tag, the other for an N-terminal VSV affinity tag. All experiments were performed in a flow-through microfluidic cell containing a reaction chamber of about 50μl volume. This chamber was sealed with the metal-coated coverslip providing a window for TIRF measurements. Two inlets at the extremities of the reaction chamber allowed to push/pull liquids through the chamber.

3. MEASUREMENTS

First, the quality of the tBLMs was verified by incubation with the anti-VSV–Cy5 (AV–Cy5) for 10min prior to the OR5 expression. TIRF images showed that the AV–Cy5 associated only at very few nanometric sites, in average about one site per $20\mu m \times 20\mu m$ area. This association was attributed to defects in the tBLM assembly, i.e. a missing top layer (imperfect vesicle spreading) or a small defect in the underlying metal coating. As these defects showed up much brighter than any other feature, they were readily identified and excluded from further analysis. Finally, it was confirmed that the incorporation of the OR5 did not affect the background.

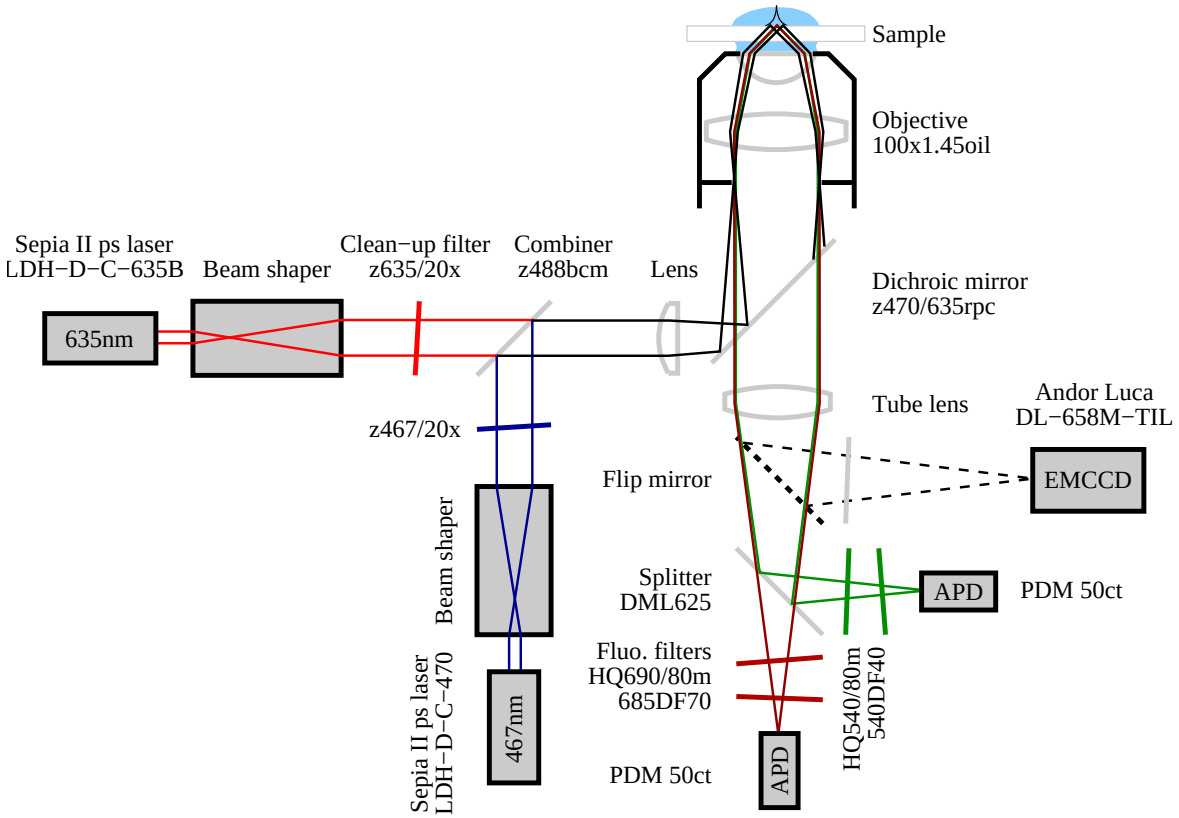

Figure 1. Dual-color TIR-FFS and imaging platform.

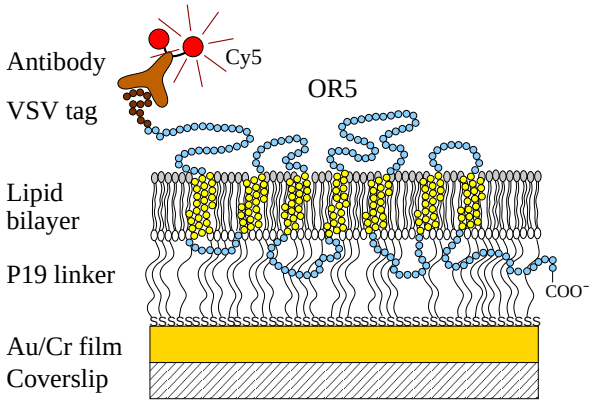

Figure 2. Solid-supported planar lipid membrane assembly with incorporated GCPR. The lipid bilayer consists of a first DMPE monolayer and a second lipid layer from spread PC vesicles. The VSV affinity tag was immunolabeled with a fluorescently labeled antibody.

In a next investigation, the vectorial incorporation of OR5 was confirmed. Figure 3 shows representative background corrected and normalized membrane images. Image (a) to (d) show the increase in the spot density and brightness with increasing expression time. Image (e) shows the negative control at 60min expression of OR5 with the VSV tag at the C' terminus. If the OR5 is fully incorporated and well oriented, this terminus is buried between the lipid membrane and the metal-coated coverslip as sketched in Fig. 2. This means, the anti-VSV–Cy5 marker should not be able to bind the tag. Indeed, only a few markers were monitored versus about 150 spots in case of the N' terminal tag. These measurements confirm the main results by Robelek et al.[2] as they show

1. the excellent quality of the artificial membrane, which is intact and nearly defect–free,
2. the absence of incompletely fused vesicles,

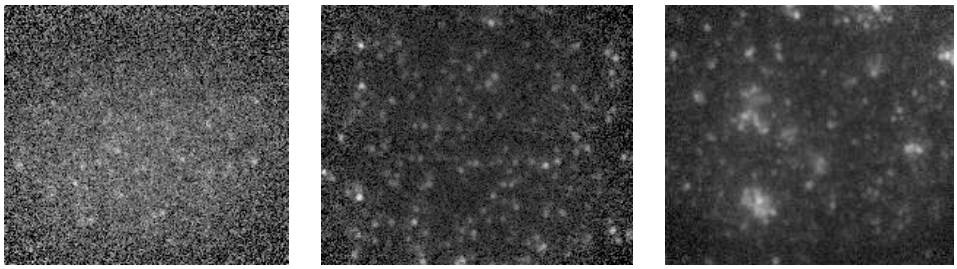

(a) 15min. (b) 30min. (c) 60min.

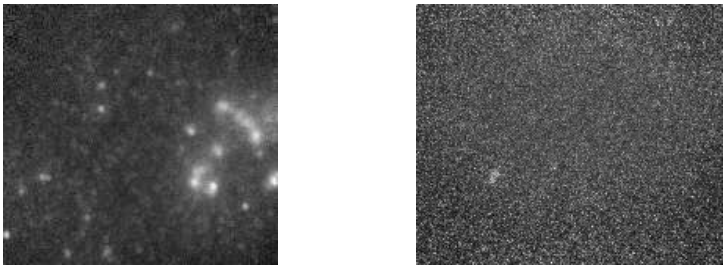

(d) 90min. (e) 60min (negative control).

Figure 3. (a)-(d) Background corrected and normalized membrane images versus expression time. The negative control (e) corresponds to 60min incorporation of OR5 with a VSV tag at the C' terminus.

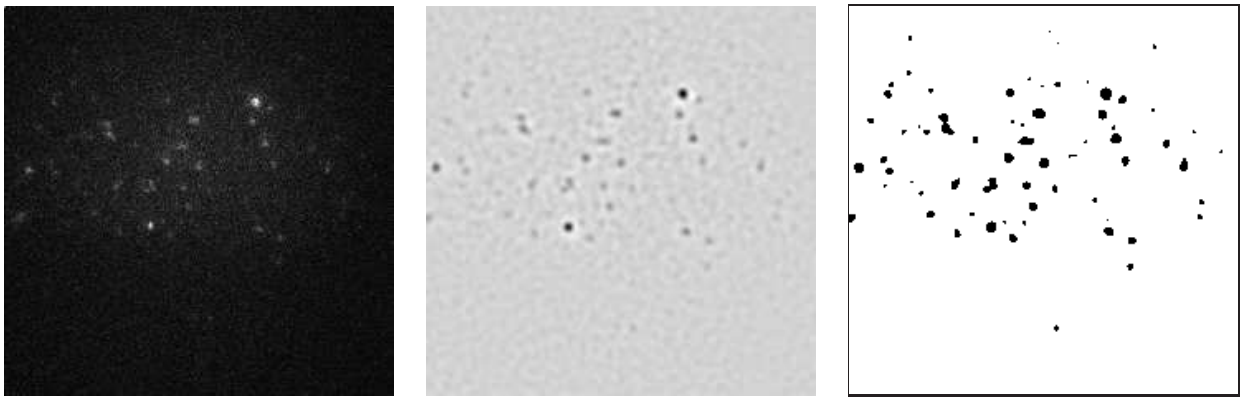

(a) OR5–AV–Cy5 complexes. (b) LoG(3) filtered image. (c) Segmented image.

Figure 4. Image segmentation analysis.

3. the vectorial incorporation and
4. the complete incorporation of OR5.

Furthermore, the OR5 incorporation density and aggregation was analyzed by means of an image segmentation as outlined in Fig. 4. The Airy density AD (an improved estimate of the spot density) was obtained with Eq. (1). Figure 5 shows the AD monitored at different expression levels obtained by varying the expression time in steps from 15min to 90min. The data points fitted in excellent agreement on a second order polynomial function of the form $\mathrm{AD}(t) = \mathrm{AD}_1(t - t_0) + \mathrm{AD}_2(t - t_0)^2$. Whether it should fit to this model curve or not is questionable, but it allowed to extract the initial increase and to extrapolate the leadtime. A leadtime t_0 of 8.0min was estimated from the fit, e.g. OR5 were fully expressed and incorporated within about 8min. With increasing expression time, the OR5 density increased linearly with $\mathrm{AD}_1 = 0.019\mu\mathrm{m}^{-2}\mathrm{min}^{-1}$ up to about 30min. In the time window of 20min to 30min, the AD variations were particularly low as a result of a homogeneous OR5 distribution in combination with an optimal image contrast and low noise. For even longer expression times, the increase of the AD slowed down with a curvature $\mathrm{AD}_2 = -7.6 \cdot 10^{-5}\mu\mathrm{m}^{-2}\mathrm{min}^{-2}$. At $t = 130$ min, the AD would achieve a maximum of about $1.2\mu\mathrm{m}^{-2}$. Taking into account that the evaluation method limits the AD to about

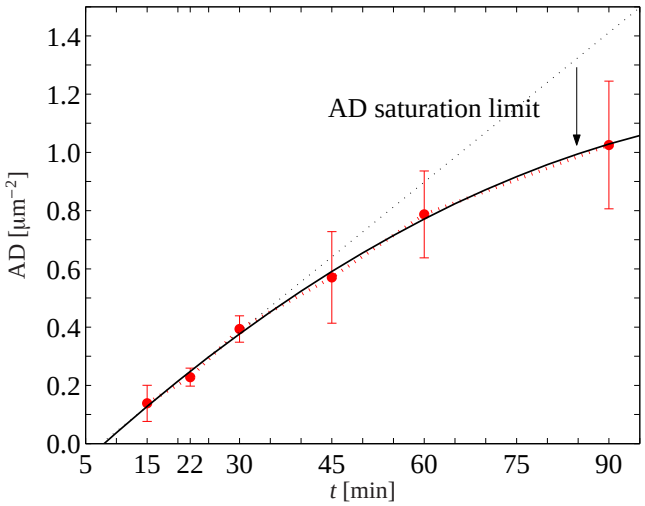

Figure 5. Airy density versus expression time t. Thin solid curve: fit on second order polynomial. The black dotted line indicates a linear increase estimated with the first three data points.

$2/3A \approx 2.5\mu m^{-2}$ (where A is the PSF cross section), a saturating model curve given by

$$\mathrm{AD}'(t) = \mathrm{AD}'_1 \frac{(t - t_0)t_s}{(t - t_0) + t_s} \tag{1}$$

was tested. This model curve matched equally well to the measured AD* for $\mathrm{AD}'_1 = 0.020\mu m^{-2}min^{-1}$ and $t_s = 135$min. Hence, the upper bound of $\mathrm{AD} < 2.7\mu m^{-2}$ was a pure artifact introduced by the evaluation method.

We concluded that the amount of expressed and incorporated OR5 increased linearly with expression time by about $0.020\mu m^{-2}min^{-1}$. The expression and incorporation of a single OR5 lasted about 8.0min, which is in good agreement with our expectations.

Next, we tried to measure the receptor mobility with FCS. The dual-color instrument with its possibility to measure in a TIRF or confocal configuration was used in the confocal mode. Thereby, premature bleaching of neighboring OR5–AV–Cy5 complexes was minimized. Figure 6a shows the intensity traces of a sequence of 5×20s measurements on incorporated OR5 (90min expression time) and a trace amount of AV–Cy5 still present after flushing the reaction chamber. The total intensity was composed of three components: a fast bleaching component (39%), a slowly bleaching component (35%), and a "non-bleaching" component (26%) consisting of background and diffusing AV–Cy5. The fast bleaching fraction had a characteristic bleaching time of about 2.0s, whereas the slow bleaching occurred at a time scale of about 36s. The fast component was attributed to photo-bleaching close to the excitation focus. The slow component was attributed to photo-bleaching within a larger area of about 1μm diameter covered by the first side lobes of the excitation field. A few intensity bursts at $t \approx 40$s were presumably due to non-specifically binding AV–Cy5. Figure 6b shows the corresponding auto-correlation curves. The strong initial bleaching resulted in a stretched decrease of the correlation amplitude. The second correlation curve represents mainly the intensity bursts with a characteristic time of 5ms to 10ms. The remaining curves are all very similar and represent the diffusion of AV–Cy5 in solution with a diffusion time $\tau_d \approx 0.15$ms. Before the last measurement, the excitation was interrupted for 150s. We observed an almost perfect on-take of the fluorescence intensity after this interruption. This effect was further investigated as it could stem (a) from diffusing OR5 in the membrane, (b) an exchange of AV–Cy5 complexes or (c) a small focus drift caused by the piezo-electric positioning device. Firstly, the focus position was verified and a small defocus was tracked and corrected. Indeed, the defocus stretched the diffusion curves shown in Fig. 6b. Secondly, remaining or dissociated AV–Cy5 were flushed with 5ml PBS. As a result, except of afterpulsing for lag times $\tau \lesssim 5\mu$s, no significant correlation amplitude was measured anymore. This result was reproduced on various membrane positions and for several samples. We concluded that if the OR5 diffuses, it must be so slow that it is below the detection limit set by photo-bleaching.

* Not shown because hardly discernable from the polynomial fit.

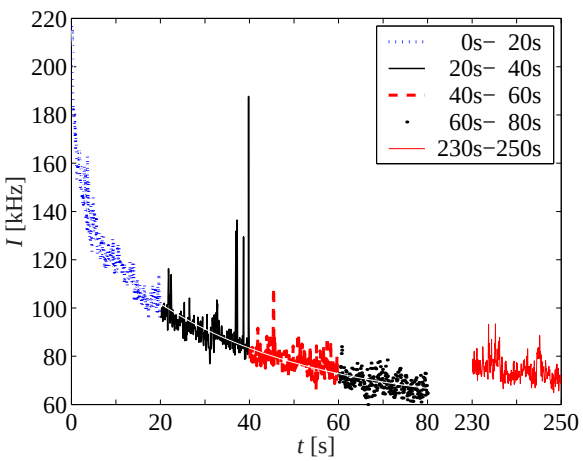

(a) Intensity traces.

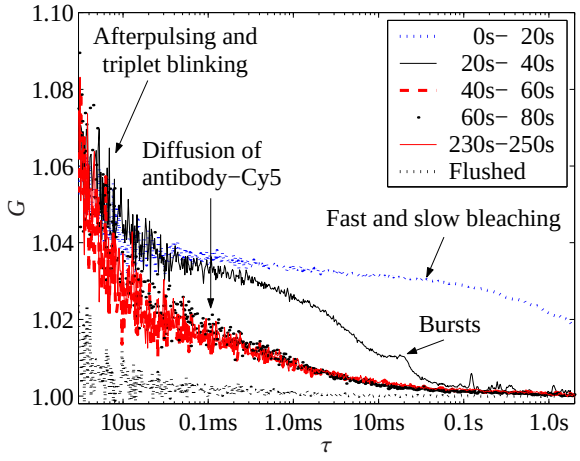

(b) Auto-correlations.

Figure 6. Intensity traces and FCS correlation curves, all taken at the same membrane position.

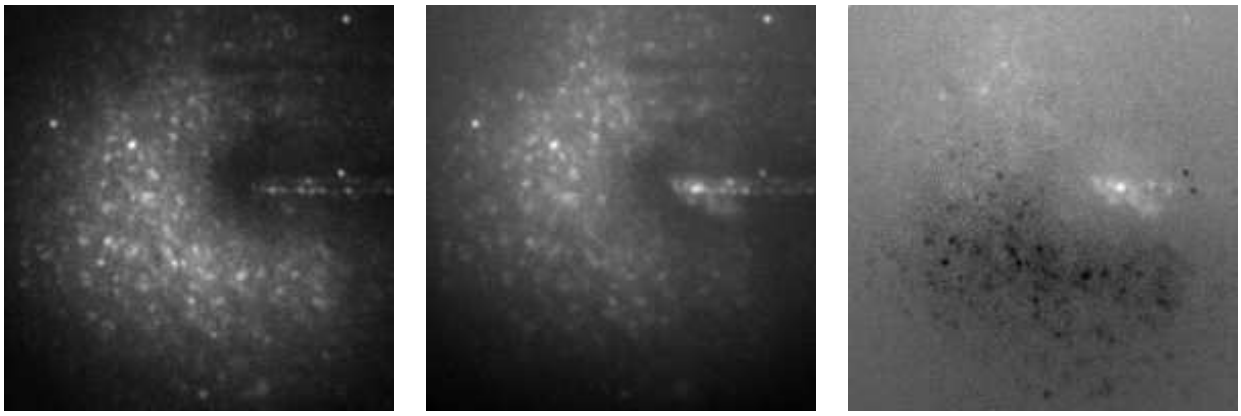

(a) Image at t = 0min. (b) Image at t = 6.5min. (c) Difference image (a)-(b).

Figure 7. FRAP experiment. A line and a ”U” were bleached and immediately imaged (a). After 6.5min, a second image was taken (b). The difference picture is shown in (c).

Additionally, slow diffusion was monitored with fluorescence recovery after photo-bleaching (FRAP). First, the Cy5 was photo-bleached along a few lines and an image was captured. Later, the same area was imaged several times for checking for recovery after bleaching. Figure 7 shows the result of these FRAP experiments. Image 7a and 7b were taken with 6.5min time lapse. The difference image 7c shows that the receptors along the single line did not move (up-right corner). The bottom darkened due to a slight focus drift, which moved the excitation area upwards. Inside the ”U”, a single spot became much brighter, whereas two spots at the right just disappeared. However, the photo-bleached features did not recover nor a ”edge” moving of the bleached pattern could be observed. This finding was confirmed with several FRAP measurements on this sample. For an expression time of 90min, we never monitored moving receptors although hundreds of CCD images were taken from several samples. Taking into account the densely packed, corkscrew-shaped P19 linker immobilizing the tBLM and winding up with the α-helices of the receptor, it would have been surprising if the OR5 diffused above the resolution limit of our instrumentation. Constrained diffusion within small domains was monitored, in particular at low expression levels favoring OR5 monomers, but the diffusion was typically limited to domains of $\lesssim \varnothing$200nm (data not shown). These findings are supported by recent studies on GPCRs in living cells and in supported membranes. For instance, Jacquier et al.[9] investigated the trafficking of the human odorant receptor OR17-40 in living cells and analyzed their mobility with single particle tracking. The OR17-40 was found to diffuse with a diffusion constant in the order of 0.02µm^2/s. About 40% were found immobile or constrained within domains of $\approx \varnothing$190nm, 49% were diffusing within domains of $\varnothing$300nm to $\varnothing$550nm and about 11% were freely diffusing. Moreover, Perez et al.[10] showed that GPCRs immobilize upon preparation of supported membranes. These membranes were prepared by detaching the upper part of a

cell membrane using a poly-L-lysine substrate. Whereas FRAP experiments performed on living cell membranes showed fast and complete recovery of bleached domains, no recovery was found on supported membranes stating that nearly all GPCRs were immobilized.

We would like to point out that single particle tracking based on TIRF images may be deceptive because the orientation of the observed fluorophore affects the shape of the PSF.[11] When imaging partially immobilized fluorophores as the AV–Cy5, the fluorophore rotation is constrained (just slow and/or limited angular distribution), such that its image appears to wiggle around if the fluorophore changes its orientation. Wiggling was frequently observed at low expression levels, but limited to an area comparable to the PSF size. The mobility of the OR5 requires further investigation, as the preliminary analysis did not differentiate between translational and rotational mobility.

4. CONCLUSIONS

In summary, the vectorial and complete insertion of OR5 receptors into an artificial tethered membrane assembly was shown. Fluorescence spectroscopy (FCS and FRAP) showed that the incorporated receptors were immobilized. The incorporation density was monitored with an image segmentation analysis. It was shown that the amount or OR5 increased with expression time up to a few receptors or aggregates per μm^2 within 90min. Moreover, the mean time for expressing and incorporating a single receptor was estimated to about 8min. Comparing OR5 distributions at different expression times revealed that the first OR5 were incorporated at random positions. Thereafter, a tendency of incorporating several OR5 side-by-side was observed, presumably due to Ribosomes staying in contact with the membrane in between two expression cycles.

ACKNOWLEDGEMENTS

We gratefully acknowledge the financial support by the European Commission within the sixth research framework program.

REFERENCES

1. R. Robelek, F. D. Stefani, W. Knoll, "Oligonucleotide hybridization monitored by surface plasmon enhanced fluorescence spectroscopy with bio-conjugated core/shell quantum dots. Influence of luminescence blinking," *phys. stat. sol. (a)* **203,** pp. 3468–3475, 2006.
2. R. Robelek, E. S. Lemker, B. Wiltschi, V. Kirste, R. Naumann, D. Oesterhelt, E.-K. Sinner, "Incorporation of *In Vitro* Synthesized GPCR into a Tethered Artificial Lipid Membrane System," *Angew. Chem. Int. Ed.* **46,** pp. 605–608, 2007.
3. S. Heyse, O. P. Ernst, Z. Dienes, K. P. Hofmann, H. Vogel, "Incorporation of Rhodopsin in Laterally Structured Supported Membranes: Observation of Transducin Activation with Spatially and Time-Resolved Surface Plasmon Resonance," *Biochem.* **37,** pp. 507–522, 1998.
4. C. Bieri, O. P. Ernst, S. Heyse, K. P. Hofmann, H. Vogel, "Micropatterned immobilization of a G protein-coupled receptor and direct detection of G protein activation," *Nature Biotech.* **17,** pp. 1105–1108, 1999.
5. Y. Lill, K. L. Martinez, M. A. Lill, B. H. Meyer, H. Vogel, B. Hecht, "Kinetics of the initial steps of G protein-coupled receptor-mediated cellular signaling revealed by single-molecule imaging," *ChemPhysChem* **6,** pp. 1633–1640, 2005.
6. N. Kahya, P. Schwille, "Fluorescence correlation studies of lipid domains in model membranes (Review)," *Mol. Membr. Biol.* **23,** pp. 29–39, 2006.
7. M. Leutenegger, H. Blom, J. Widengren, C. Eggeling, M. Gösch, R. A. Leitgeb, T. Lasser, "Dual-color Total Internal Reflection Fluorescence cross-Correlation Spectroscopy," *J. Biomed. Opt.* **11,** 040502, 2006.
8. M. Leutenegger, *Single molecule detection on surfaces*, chapt. 3, EPFL Ph.D. thesis no. 3854, Lausanne, 2007.
9. V. Jacquier, M. Prummer, J.-M. Segura, H. Pick, H. Vogel, "Visualizing odorant receptor trafficking in living cells down to the single-molecule level," *PNAS* **103,** pp. 14325–14330, 2006.
10. J.-B. Perez, J.-M. Segura, D. Abankwa, J. Piguet, K. L. Martinez, H. Vogel, "Monitoring the diffusion of single heterotrimeric G proteins in supported cell-membrane sheets reveals their partitioning into microdomains," *J. Mol. Biol.* **363,** pp. 918–930, 2006.
11. P. Dedecker, B. Muls, J. Hofkens, J. Enderlein, J. Hotta, "Orientational effects in the excitation and de-excitation of single molecules interacting with donut-mode laser beams," *Opt. Express* **15,** pp. 3372–3383, 2007.